A reduced model for Eady's problem

Xihan Zhang (u6592339)

04/11/2018

1 Eady's problem

Eady's problem is a baroclinic instability model in which the mean flow has uniform zonal velocity shear and is uniformly stratified.It also neglects variation of Coriolis and vertical velocity. These assumptions are expressed as:

- Coriolis effect is invariable (f-plane, Coriolis coefficient is a constant f_0 over the whole domain)
- Fluid is uniformly stratified, so buoyancy frequency N^2 is constant ($N^2 = \frac{g}{\theta}\frac{d\theta}{dz}$, where g is acceleration of gravity and θ is potential temperature of atmosphere), which is an appropriate approximation for troposphere
- Fluid has uniform velocity shear ($U = \Lambda z = \frac{U_0}{H} z$)
- The bottom and surface are flat and rigid ($w = 0$)

1.1 Basic state

Eady's model is under the approximation of Quasi-geostrophic motion,

$$\begin{aligned} &\frac{\partial q}{\partial t} + \mathbf{u}\nabla q = 0, \qquad 0 < z < H \\ &\frac{\partial b}{\partial t} + \mathbf{u}\nabla b = 0, \qquad z = 0 \quad and \quad H \end{aligned} \tag{1}$$

where buoyancy (b), velocities (u,v) and potential vorticity (q) can be written in terms of streamfunction Ψ.

$$\begin{aligned} b &= f_0 \frac{\partial \Psi}{\partial z} \\ u &= -\frac{\partial \Psi}{\partial y} \\ v &= \frac{\partial \Psi}{\partial x} \\ q &= f_0 + (\frac{\partial^2}{\partial x^2} + \frac{\partial^2}{\partial y^2} + \frac{f_0^2}{N^2}\frac{\partial^2}{\partial z^2})\Psi \end{aligned} \tag{2}$$

Basic state of streamfunction in Eady's model is $\Psi = -\Lambda yz$, giving the basic state of potential vorticity (Q) and buoyancy (B):

$$\begin{aligned} Q &= \nabla^2\Psi + \frac{H^2}{L_d^2}\frac{\partial}{\partial z}(\frac{\partial \Psi}{\partial z}) = 0 \\ B &= f_0\frac{\partial \Psi}{\partial z} = -f_0\Lambda y \end{aligned} \tag{3}$$

1.2 Equations of perturbation

Induce a 2-D perturbation $\Psi' = \Psi'(x, z, t)$ to (1) and linearise the equations to obtain equations of motion for perturbation:

$$(\frac{\partial}{\partial t} + \Lambda H\frac{\partial}{\partial x})\frac{\partial}{\partial z}\Psi'_+ - \Lambda\frac{\partial}{\partial x}\Psi'_+ = 0 \quad , z = H \tag{4}$$

$$(\frac{\partial}{\partial t} + \Lambda z\frac{\partial}{\partial x})(\frac{\partial^2}{\partial x^2} + \frac{f_0}{N^2}\frac{\partial^2}{\partial z^2})\Psi' = 0 \quad , 0 < z < H \tag{5}$$

$$\frac{\partial}{\partial t}\frac{\partial}{\partial z}\Psi'_- - \Lambda\frac{\partial}{\partial x}\Psi'_- = 0 \quad , z = 0 \tag{6}$$

where Ψ'_+ and Ψ'_- denote streamfunction at top and bottom respectively.
After non-dimensionalisation ($z = H\tilde{z}$, $x = \frac{NH}{f_0}\tilde{x}$, $t = \frac{N}{\Lambda f_0}\tilde{t}$),

$$(\frac{\partial}{\partial \tilde{t}} + \frac{\partial}{\partial \tilde{x}})\frac{\partial}{\partial \tilde{z}}\tilde{\Psi}'_+ - \frac{\partial}{\partial \tilde{x}}\tilde{\Psi}'_+ = 0 \quad , \tilde{z} = 1 \tag{7}$$

$$\underbrace{(\frac{\partial}{\partial \tilde{t}} + \tilde{z}\frac{\partial}{\partial \tilde{x}})}_{\text{i}}\underbrace{(\frac{\partial^2}{\partial \tilde{x}^2} + \frac{\partial^2}{\partial \tilde{z}^2})}_{\text{ii}}\tilde{\Psi}' = 0 \quad , 0 < \tilde{z} < 1 \tag{8}$$

$$\frac{\partial}{\partial \tilde{t}}\frac{\partial}{\partial \tilde{z}}\tilde{\Psi}'_- - \frac{\partial}{\partial \tilde{x}}\tilde{\Psi}'_- = 0 \quad , \tilde{z} = 0 \tag{9}$$

Since equations are homogeneous in terms of x then solution is of the form

$$\Psi'(x, z, t) = \hat{\Psi}(z, t)e^{ikx} \tag{10}$$

Energy of perturbation is

$$\begin{aligned} E =& \int \frac{1}{2}(u^2 + \frac{b^2}{N^2})dxdz \\ =& \frac{H^2\Lambda^2}{4}\int (|\frac{\partial \hat{\Psi}}{\partial \tilde{z}}|^2 + k^2|\hat{\Psi}|^2)d\tilde{z} \end{aligned} \tag{11}$$

This linear system can be written as

$$\frac{d}{dt}\Psi' = \mathbb{A}_{\mathbb{M}}\Psi' \tag{12}$$

2 Edge waves

2.1 Physical interpretation of baroclinic instability

To interpret Eady's model physically, we first consider a stratification in two directions (zonal x and vertical z). Assume the flow is hydrostatic and geostrophic, therefore:

$$\begin{aligned} 0 &= -\frac{\partial p}{\partial z} - \rho g \\ -fv &= -\frac{1}{\rho_0}\frac{\partial p}{\partial x} \end{aligned} \tag{13}$$

from which we can obtain

$$\frac{\partial v}{\partial z} = -\frac{g}{\rho_0 f}\frac{\partial \rho}{\partial x} \tag{14}$$

This equation describes the relation between vertical velocity gradient and zonal density gradient, which is known as 'thermal wind equation'. The basic state of Eady's problem, constant vertical velocity gradient implies horizontal density gradient (equivalent to temperature or buoyancy gradient in this model), is shown in Fig. 1

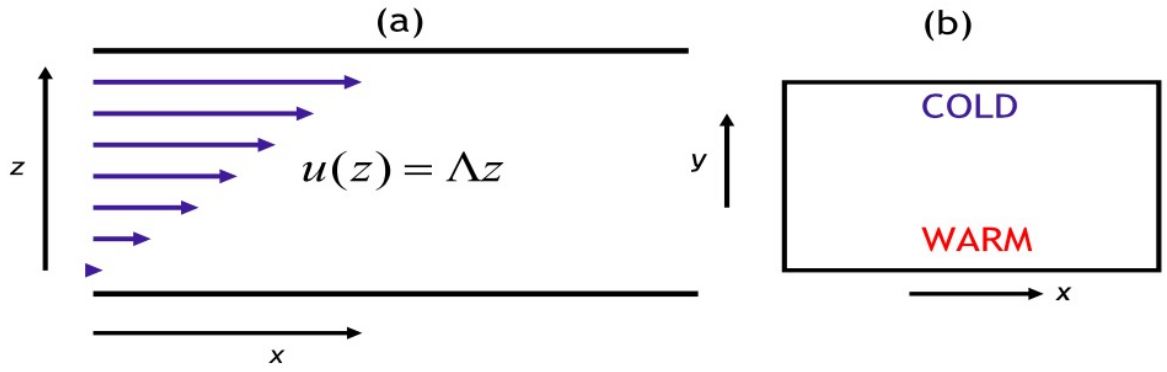

Figure 1: Basic state of Eady problem.(a) Zonal velocity profile (b) Horizontal temperature gradient. From Simpson (2011).

This horizontal gradient of temperature can be considered as a simplification of atmosphere in North Hemisphere with polar in the north and equator in the south.

By solving $(ii) = 0$ in (8), there are two solutions satisfying the equation for interior flow:

$$\Psi'(x,z,t) = \alpha(t) e^{\pm \frac{Nk}{f_0} z} e^{ikx} \tag{15}$$

where

$$\hat{\Psi} = \alpha(t) e^{\pm \frac{Nk}{f_0} z} \tag{16}$$

Consider waves that only exist at two boundaries by constructing solution(16). To ensure both of them decaying into the interior, we assume top wave as

$$\hat{\Psi}_{top} = e^{\frac{Nk}{f_0}(z-H)} e^{-ikc_{top}t} \tag{17}$$

and the bottom wave is

$$\hat{\Psi}_{bottom} = e^{-\frac{Nk}{f_0}z} e^{-ikc_b t} \tag{18}$$

where c_{top} and c_b are top and bottom wave speed respectively. Substitute top wave solution into(4), we can get the top wave speed is $c_{top} = \Lambda H - \frac{f_0 \Lambda}{kN}$. Similarly, plug bottom wave solution into (6), and bottom wave speed is $c_b = \frac{f_0 \Lambda}{kN}$. To gain instability, one of the necessary conditions is that bottom wave and top wave need to move with the same wave speed, which makes $c_b = c_{top} = \frac{1}{2}\Lambda H = \frac{1}{2}U_0$. The interpretation for instability through edge wave solution as follows.

We first consider the top wave, shown in Fig. 2

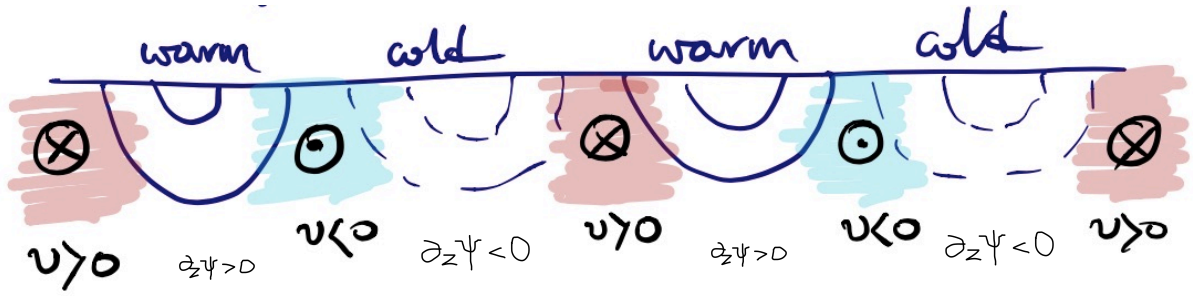

Figure 2: Top wave diagram,⊗ is the direction pointing into the paper,which carries warm water (red shadows). ⊙ is the direction pointing out of the paper which carries cold water (blue shadows). Solid line represents contours of positive streamfunction while dash lines represents negative ones. From Navid C Constantinou (personal communications)

Since buoyancy can be expressed in terms of streamfunction $b = f\frac{\partial \Psi}{\partial z}$, positive vertical gradient of Ψ gives us positive buoyancy, indicating warm anomaly and negative vertical gradient stands for cold anomaly. As for zonal gradient of streamfunction, $v = \frac{\partial \Psi}{\partial x}$, therefore positive zonal gradient implies positive meridional velocity (pointing in to the paper) while negative zonal gradient the other direction (pointing out of the paper). Thus, at the top, warm anomaly is the centre for anticyclone and cold anomaly is the centre for cyclone. In addition, due to the temperature gradient of basic state, when $v > 0$, flow carries warm water from 'equator', while $v < 0$, flow brings cold water from 'polar' to 'equator'. Fig. 3 shows the similar pattern for bottom wave. Warm anomaly is associated with cyclones while cold anomaly is the centre of anticyclones.

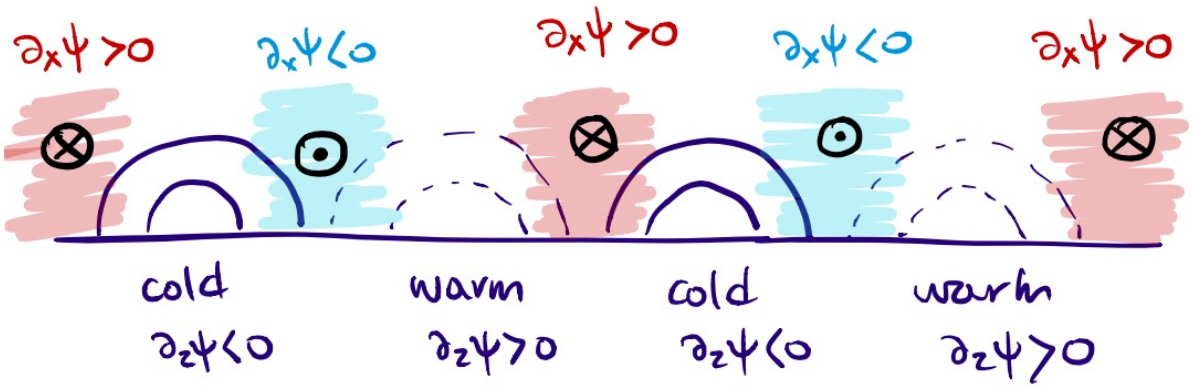

Figure 3: Bottom wave diagram.From Navid C Constantinou (personal communications)

As both of edge waves decay in interior, the strength of meridional velocity also decreases as they propagate to the interior. If $\frac{Nk}{f_0}$ is large enough, edge waves are trapped at boundaries and they cannot reach the other boundary. However, for smaller $\frac{Nk}{f_0}$, top (bottom) wave can propagate to the bottom (top) thereby interacting with bottom (top) edge wave. The most unstable state that the two edge waves can produce is shown in Fig. 4.

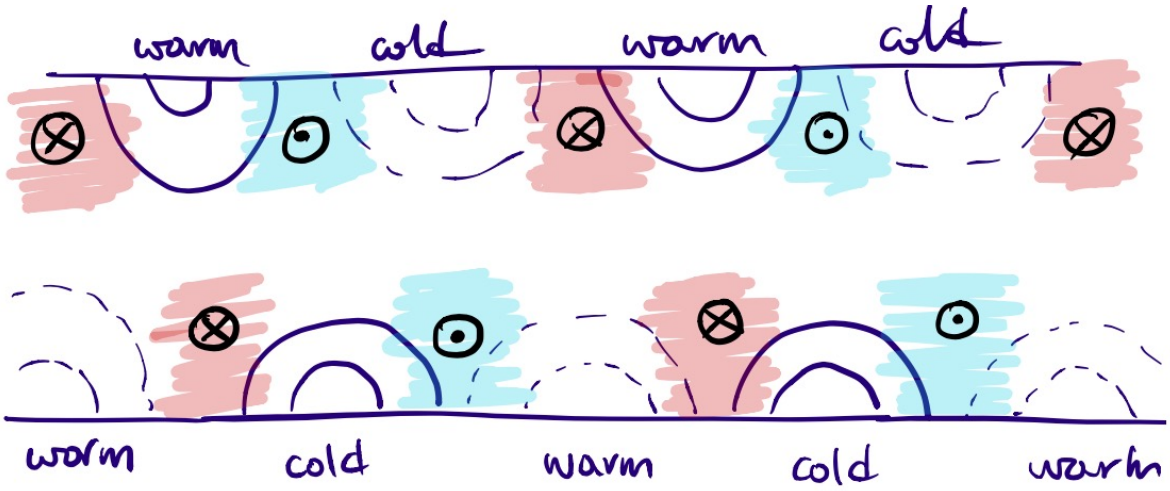

Figure 4: Interaction between edge waves. From Navid C Constantinou (personal communications)

This configuration of edge waves allows meridional velocity at the bottom which carries warm (cold) water to propagate to the top. This results in the initial warm (cold) anomaly at the top even warmer (colder). The same process also applies to the propagation from top to bottom.

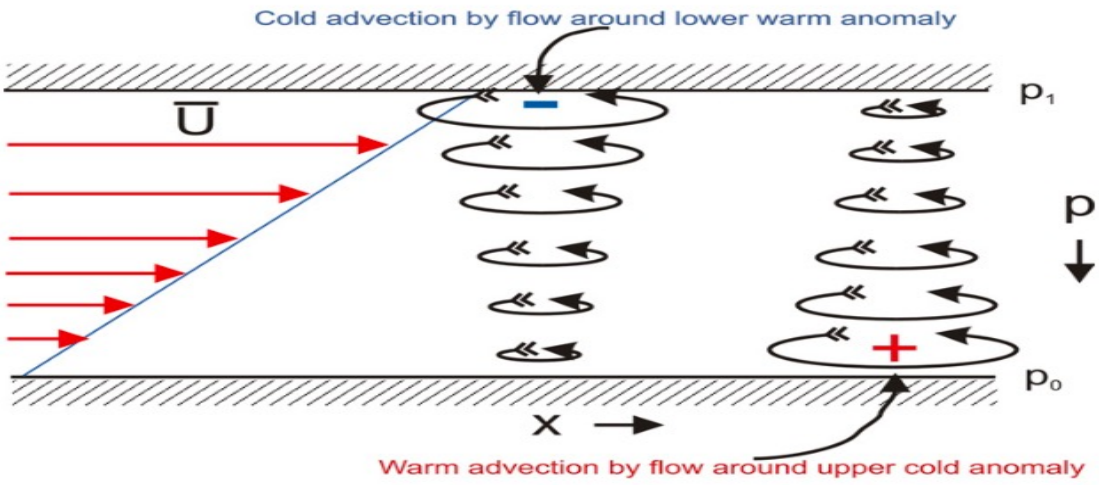

Figure 5: Wave propagation between two edges. From Emanuel (2009)

This explains the unstable mode streamline we saw before, shown in Fig. 6(a). Similarly, stable mode is obtained when edge waves always suppress initial anomalies at the other boundary (Fig. 6(b)).

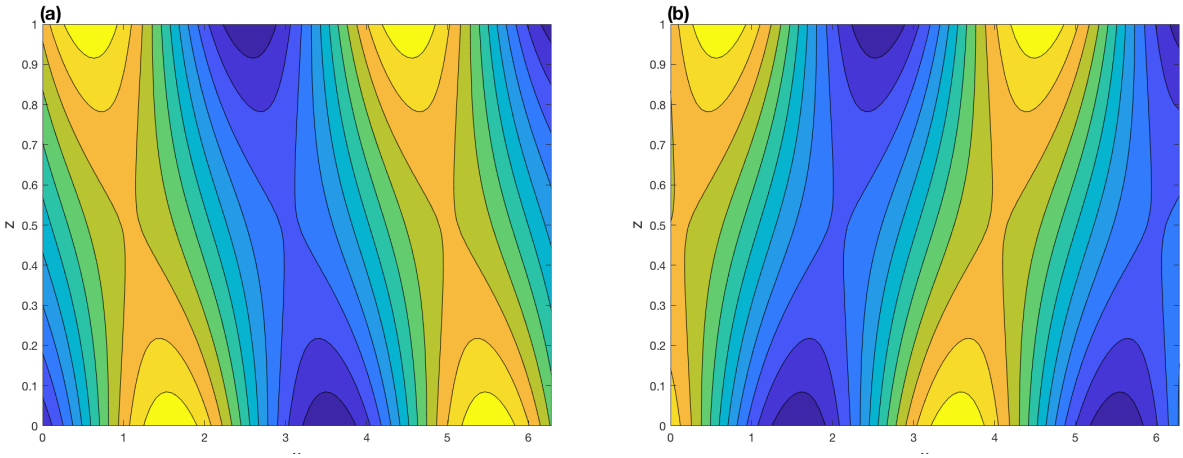

Figure 6: (a) unstable mode (b) stable mode of Eady's problem

2.2 A reduced system for Eady problem

In last section, by making $(ii) = 0$ in (8) and constructing waves at two boundaries which decay in interior, we obtained two edge wave solutions $\hat{\Psi}_{top} = e^{-\frac{Nk}{f_0}(H-z)}$ and $\hat{\Psi}_{bottom} = e^{-\frac{Nk}{f_0}z}$. Now we assume the solution

is a linear combination of top wave and bottom wave:

$$\begin{aligned}\Psi' =&\hat{\Psi}(z,t)e^{ikx}\\ =&(\alpha_1(t)\Psi_{bottom}+\alpha_2(t)\Psi_{top})e^{ikx}\\ =&(\alpha_1(t)e^{-\frac{Nk}{f_0}z}+\alpha_2(t)e^{\frac{Nk}{f_0}(z-H)})e^{ikx}\\ =&(\alpha_1 e^{-K\tilde{z}}+\alpha_2 e^{K(\tilde{z}-1)})e^{iK\tilde{x}}\end{aligned} \tag{19}$$

where the last line is the expression after nondimensionalization and K is non-dimensional wave number $K=\frac{Nk}{f_0}$. Plug this solution into (7) and (9), then we can get a reduced system:

$$\frac{d}{dt}\begin{bmatrix}\alpha_1\\ \alpha_2\end{bmatrix}=\underbrace{\begin{bmatrix}-e^{-K} & 1\\ -1 & e^{-K}\end{bmatrix}^{-1}\begin{bmatrix}(i+iK)e^{-K} & i-iK\\ i & ie^{-K}\end{bmatrix}}_{\mathbb{C}}\begin{bmatrix}\alpha_1\\ \alpha_2\end{bmatrix} \tag{20}$$

Denote $\alpha=\begin{bmatrix}\alpha_1\\ \alpha_2\end{bmatrix}$, the system becomes

$$\frac{d}{dt}\alpha=\mathbb{C}\alpha \tag{21}$$

Energy per wave length of this system:

$$E(t)=\hat{\Psi}_+^*\frac{\partial}{\partial\tilde{z}}\hat{\Psi}_+-\hat{\Psi}_-^*\frac{\partial}{\partial\tilde{z}}\hat{\Psi}_- \tag{22}$$

$$E(t)=\begin{bmatrix}\alpha_1^* & \alpha_2^*\end{bmatrix}\underbrace{\begin{bmatrix}-K(e^{-2K}+1) & 0\\ 0 & -K(e^{-2K}+1)\end{bmatrix}}_{\mathbb{M}}\begin{bmatrix}\alpha_1\\ \alpha_2\end{bmatrix} \tag{23}$$

Make a new variable $\beta=\mathbb{M}^{\frac{1}{2}}\alpha$ and a new matrix $\mathbb{C}_{\mathbb{M}}=\mathbb{M}^{-\frac{1}{2}}\times\mathbb{C}\times\mathbb{M}^{\frac{1}{2}}$ Now energy can be written as $E(t)=(\beta,\beta)$ and (21) becomes

$$\frac{d}{dt}\beta=\mathbb{C}_{\mathbb{M}}\beta \tag{24}$$

Conduct eigenanalysis to this 2×2 system, maximum real part of eigenvalue is the 'approximated' growth rate. Comparison between this approximation and analytical growth rate is plotted in Fig. 7.

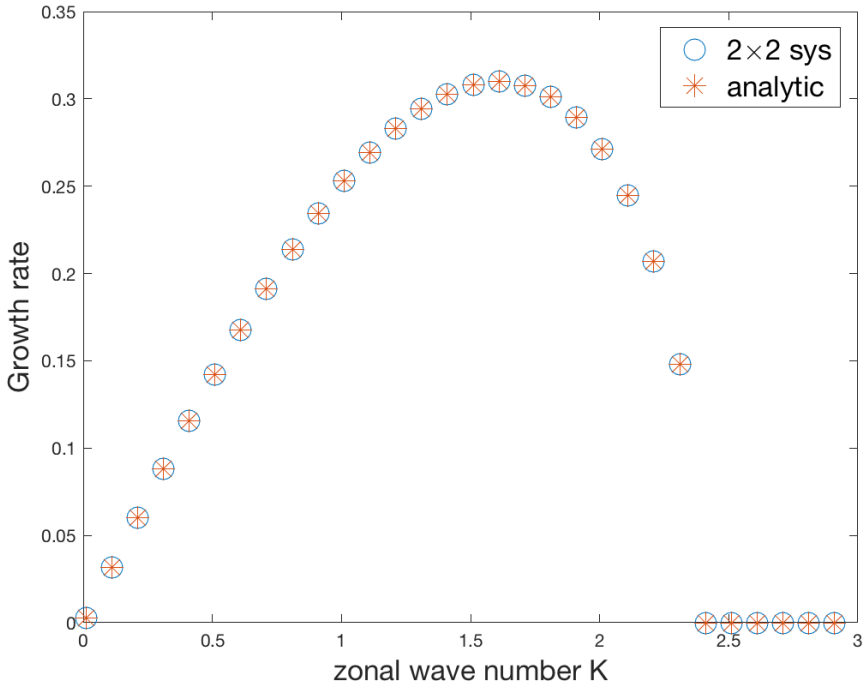

Figure 7: Comparison between analytical and approximate growthrate

They overlap each other exactly and it makes sense because analytical solution is derived on condition that $\Lambda z - c \neq 0$, i.e. (i) in (5) $\neq 0$ and eigenanalysis of this 2×2 system only gives us most stable and most unstable mode in terms of modal instability. Consistent with interpretation of edge wave, small K ($K < 2.4$) allows edge waves propagate to the other boundary and interact with each other, enabling modal instability. The maximum instability occurs when K=1.6. Take most modally unstable situation (K=1.6) for example, solve eigenproblem of this coefficients matrix and substitute maximum real part of eigenvalues into the linear combination to get corresponding streamfunction. Results are plotted in Fig. 8.

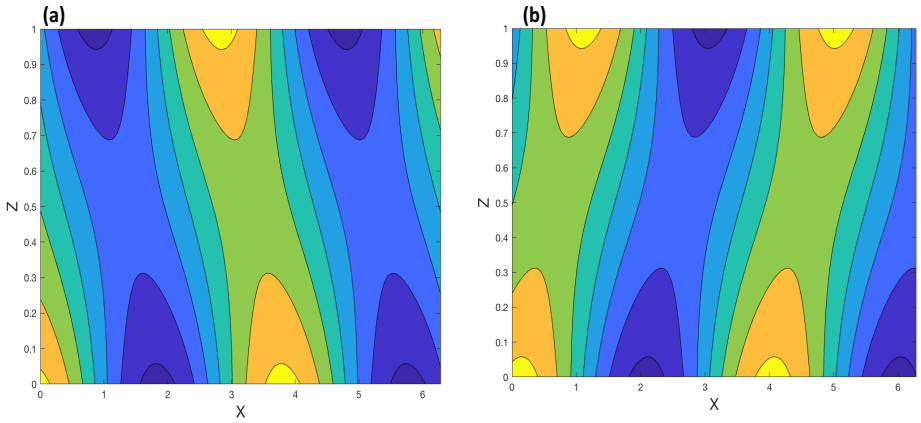

Figure 8: Eidgenmode of reduced system when K=1.6

It can be seen that two modes for maximum modal instability gives us unstable mode and stable mode which are similar with those two modes for full system(Fig. 6).

3 Results: Optimal initial condition for reduced system

In this section, we seek for optimal initial condition to excite this reduced system for larger energy growth than the eigenmodes. We will explore both modally stable and unstable situations. For each situation, take K=1.6 and K=2.6 for example respectively and compare the energy growth with full system. According to generalised stability theory, when linear operator for the system $\mathbb{A}_{\mathbb{M}}$ is non-normal, eigenvectors for different operators can produce maximum energy growth at different time (Table 1).

Eigenvector of Operator	Maximum energy growth at time
$\mathbb{A}_{\mathbb{M}} + \mathbb{A}_{\mathbb{M}}^{\dagger}$	instantaneous (small time)
$\mathbb{A}_{\mathbb{M}}^{\dagger}$	infinite time
$e^{\mathbb{A}_{\mathbb{M}}^{\dagger} t_* + \mathbb{A}_{\mathbb{M}} t_*}$	time t_*

Table 1: Initial conditions that produce maximum energy at different time

3.1 Modally unstable (K=1.6)

Linear operator for reduced system is $\mathbb{C}_{\mathbb{M}}$, the eigenvectors of which are stable and unstable model shown in Fig. 8. Choose $t_* = 5$, energy growth ($\frac{E(t)}{E(0)}$) is plotted in Fig. 9.

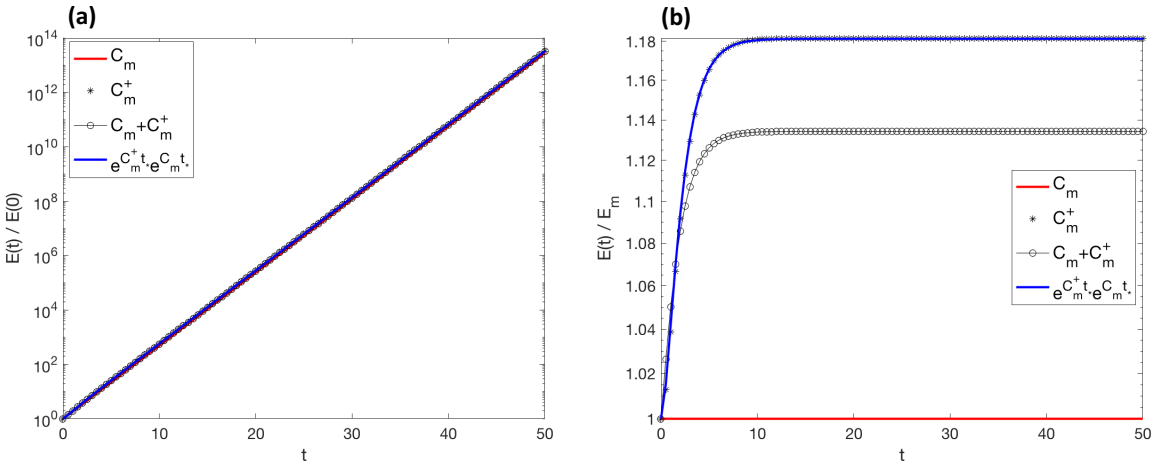

Figure 9: Energy growth comparison for different initial conditions in reduced system (a): ratio between energy evolution and initial energy for each initial condition (b): ration between energy evolution for each initial condition and energy evolution initialised by the unstable mode (E_m)

Fig. 9 (a) shows that the difference of energy growth perturbed by various initial conditions is not obvious.

To quantify the changes in energy excited by these eigenvectors compared with energy growth for unstable mode, (b) displays the ratio between them. Eigenmode of $\mathbb{C}_{\mathbb{M}} + \mathbb{C}_{\mathbb{M}}^{\dagger}$ give us the maximum energy growth (slightly larger than other eigenmodes) over small time and it has about 13% larger energy than the unstable mode eventually. The optimal initial condition at $t_* = 5$, overlap with the infinite optimal initial condition almost all the time, producing about 20% more energy than unstable mode. Corresponding streamfunctions for each initial condition are shown in Fig. 10.

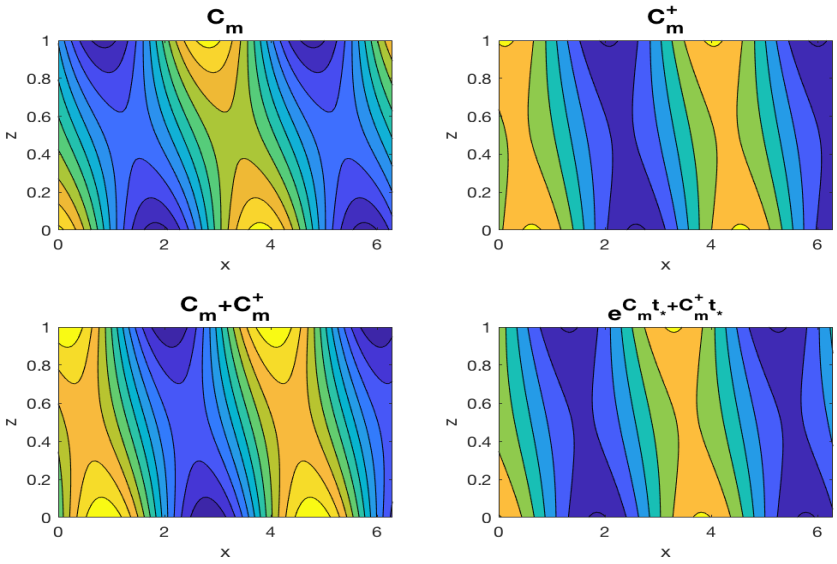

Figure 10: Initial streamfunctions corresponding to different operators in reduced system

Fig 10 indicates that all these initial conditions satisfy the configuration of two edge waves to gain instability and the structure does not change significantly among them. Now we compare this reduced system with full system.

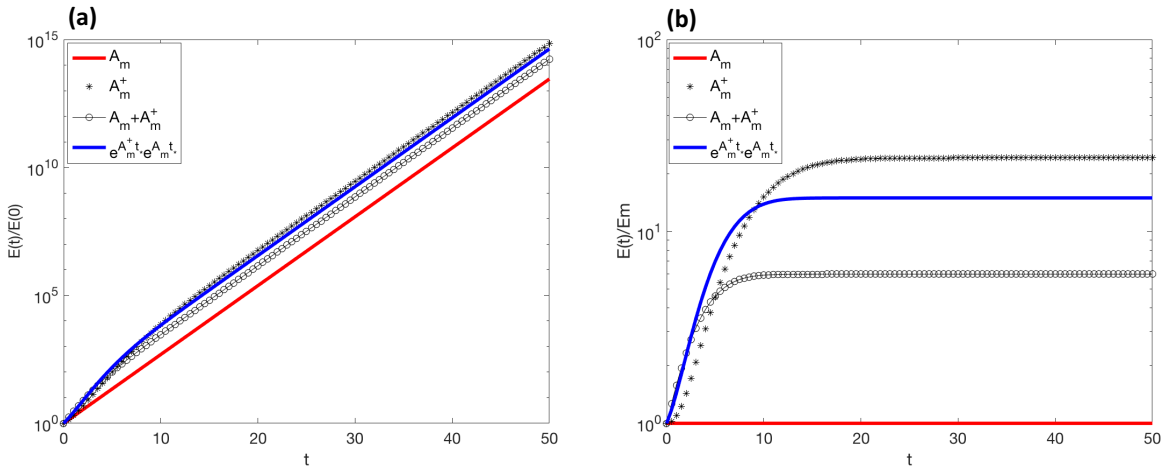

Figure 11: Energy growth comparison for different initial conditions in full system (a): ratio between energy evolution and initial energy for each initial condition (b): ration between energy evolution for each initial condition and energy evolution initialised by the unstable mode (E_m)

Fig. 11 shows the unstable mode still grows at the lowest speed and eigenmode of $\mathbb{A}_{\mathbb{M}} + \mathbb{A}_{\mathbb{M}}^{\dagger}$ generates maximum energy growth for small time. When $t = 5$ eigenmode of $e^{\mathbb{A}_{\mathbb{M}}^{\dagger} t_* + \mathbb{A}_{\mathbb{M}} t_*}$ gives the largest energy among these initial conditions while eigenmode for $\mathbb{A}_{\mathbb{M}}^{\dagger}$ produces maximum energy growth for infinite time. Notably, energy for optimal modes can reach around as much as 20 times larger than the unstable mode.
Streamfunctions of initial condition are shown in Fig. 12

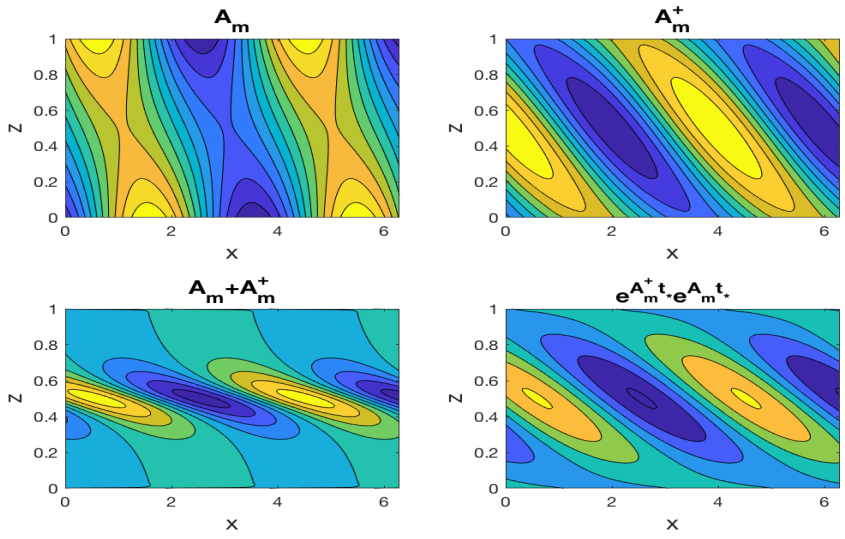

Figure 12: Initial streamfunctions corresponding to different operators in full system

The unstable mode for the full system (upper left in Fig. 12) is similar with that in reduced system and the pattern can be explained by edge waves. However, optimal initial conditions for various time have a lot structures in the interior which are very different from the unstable mode.

3.2 Modally stable

When K=2.6, the system is modally stable, i.e. all the eigenmodes for the linear operator have zero growth rate (real part of eigen value is zero). Compute energy growth for optimal initial conditions (Fig. 13)

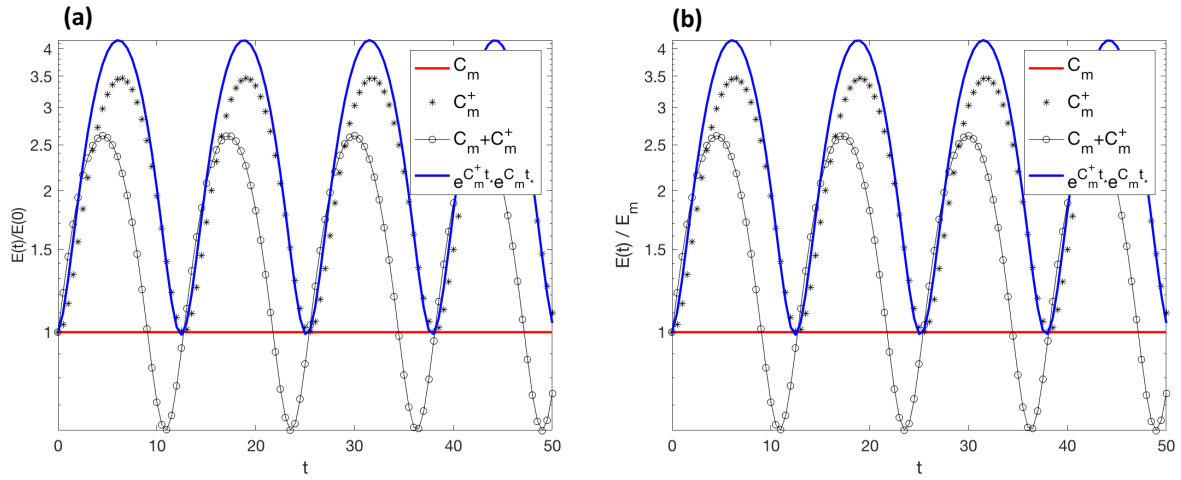

Figure 13: Energy growth comparison for different initial conditions in reduced system (a): ratio between energy evolution and initial energy for each initial condition (b): ration between energy evolution for each initial condition and energy evolution initialised by the unstable mode (E_m)

Eigenmode gives us constant energy therefore (a) and (b) are the same in Fig. 13. Although eigen mode shows no energy growing with time, there are still transient energy increase for optimal initial conditions and the largest energy can sometime reach 4 times of the eigen mode. Structure for the corresponding streamfunctions are shown in Fig. 14.

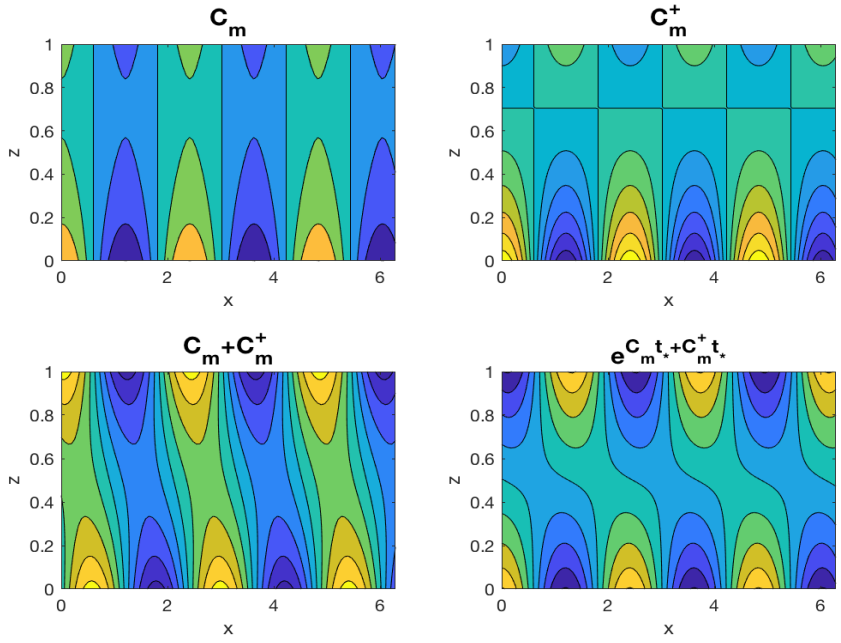

Figure 14: Initial streamfunctions corresponding to different operators in reduced system

Eigenmode of $\mathbb{C}_{\mathbb{M}}$ (upper left in Fig. 14) has no growth rate and will propagate zonally without interaction between two edge waves. Eigenmode of $\mathbb{C}_{\mathbb{M}} + \mathbb{C}_{\mathbb{M}}^{\dagger}$ has the structure of unstable mode and the eigenmode for $e^{\mathbb{C}_{\mathbb{M}}^{\dagger} t_* + \mathbb{C}_{\mathbb{M}} t_*}$ is slightly different but still satisfy the configuration of edge waves discussed in section 2.

Now we look at the modally stable full system.

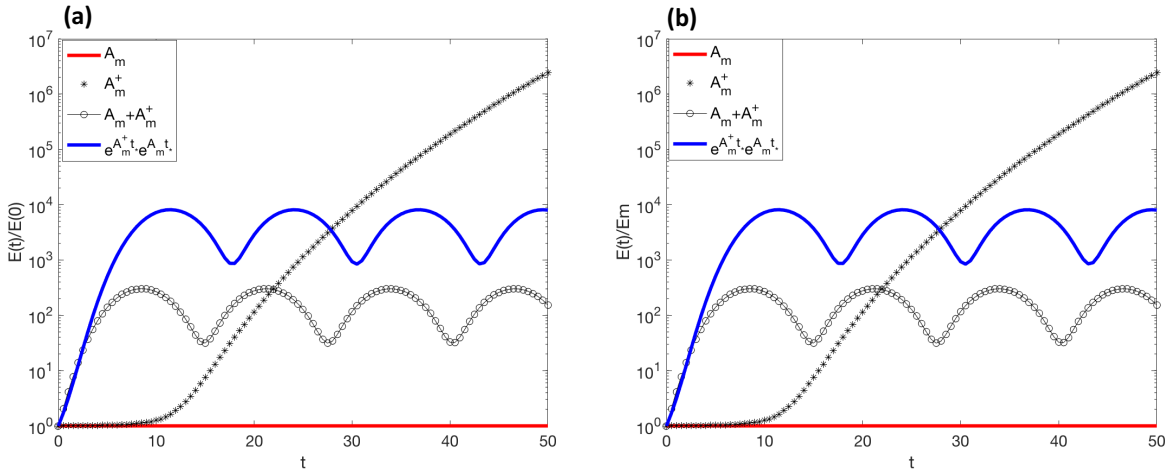

Figure 15: Energy growth comparison for different initial conditions in full system (a): ratio between energy evolution and initial energy for each initial condition (b): ration between energy evolution for each initial condition and energy evolution initialised by the unstable mode (E_m)

Energy does not grow for eigenmode of $\mathbb{A}_{\mathbb{M}}$ but eigenmodes for other operators can generate transient energy

which sometime reach 10^6 additional energy within $t = 50$. The energy excited by eigenvector of $e^{\mathbb{A}_{\mathbb{M}}^{\dagger} t_* + \mathbb{A}_{\mathbb{M}} t_*}$ will keep growing after $t = 50$ which is not plotted in this figure, but we can already gain the sense that full system has much more non-modal instability than the reduced system. As before, we plot the corresponding initial conditions (Fig. 16).

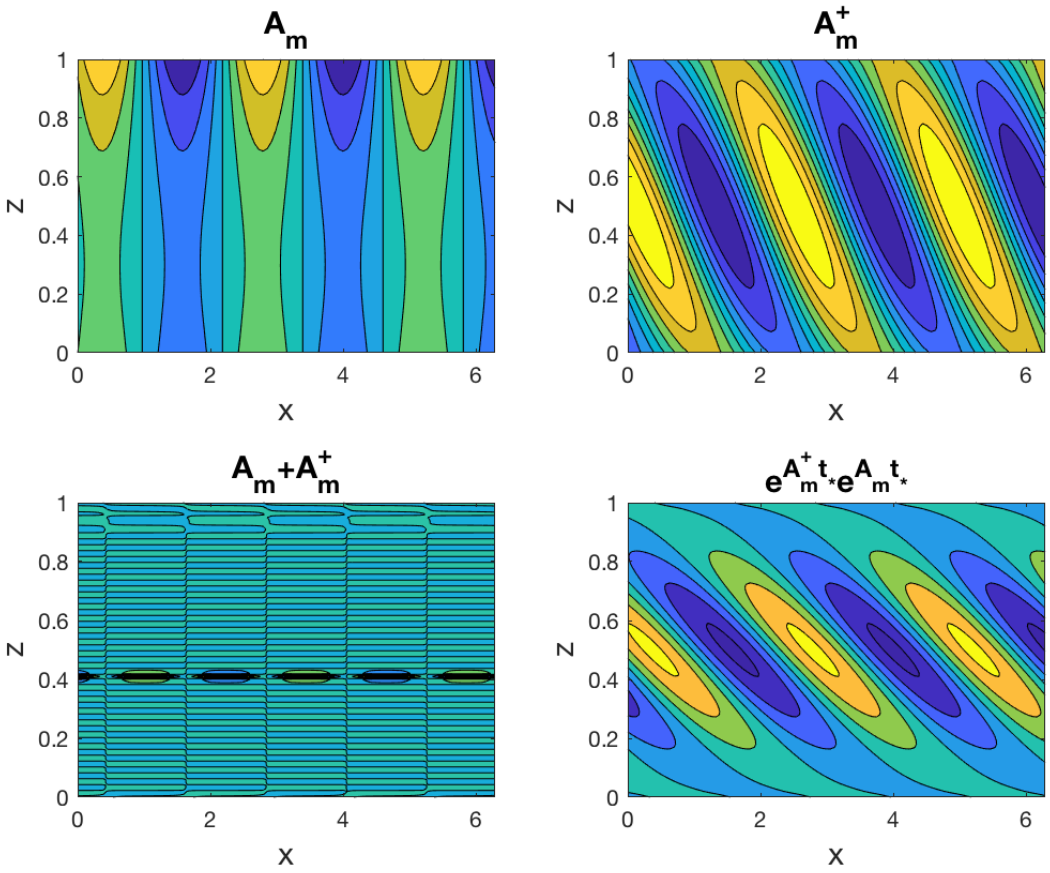

Figure 16: Initial streamfunctions corresponding to different operators in reduced system

Structures for the optimal initial conditions are constructed for the interior which can not simply explained by edge waves.

It is obvious that full system can have much more transient energy grow than reduced system and this is because the linear operator for the full system $\mathbb{A}_{\mathbb{M}}$ is more 'non-normal' than that for the reduced system $\mathbb{C}_{\mathbb{M}}$.

4 Discussion: Continuous Spectrum

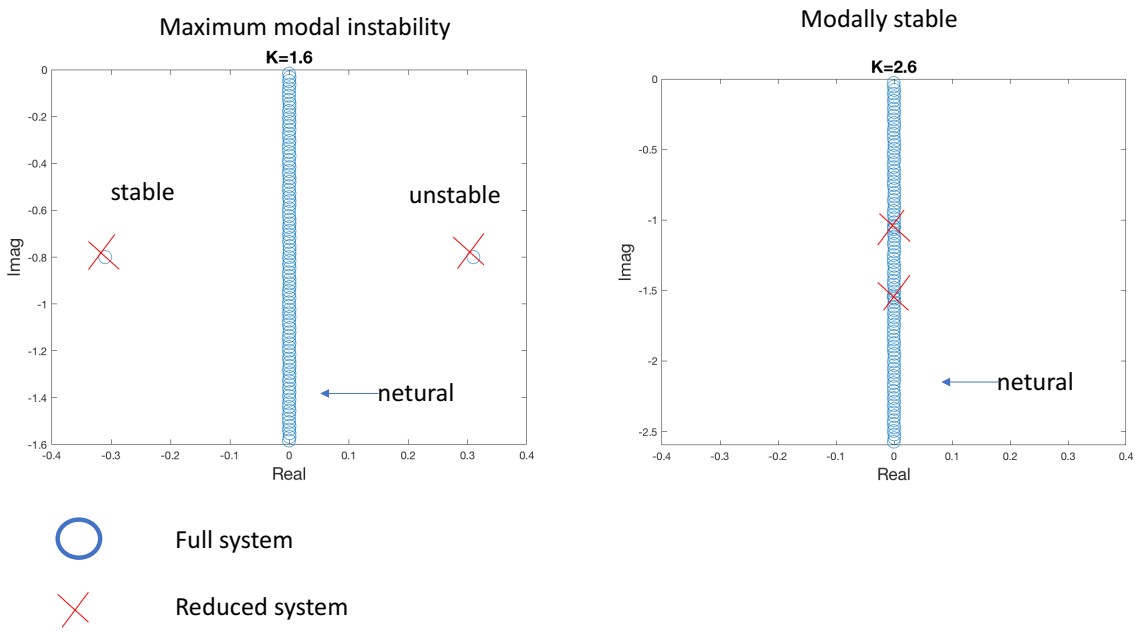

Figure 17: continuous mode spectrum

Since reduced system only solve (ii) in (8), it only has two eigenmodes to combine with. In fact, full system has more than these two eigen modes. Fig. 17 shows eigenvalues of two systems in two situations. When K=1.6 (Fig 17(a)), there are one stable mode and one unstable mode in reduced system. In contrast, full system has a straight line in the middle consist of eigenvalues with no real parts but continuous imaginary parts. Since their real parts are zero, they do not grow nor decay (netrual modes). These modes come from (i) in (8). Suppose the form of solution is $\Psi' = \phi(z)e^{ik(x-ct)}$,(5) becomes

$$\underbrace{k(\Lambda z - c)}_{\text{i}}\underbrace{[-k^2\phi + \frac{H^2}{L_d^2}\frac{\partial^2\phi}{\partial z^2}]}_{\text{ii}} = 0 \quad , 0 < z < H \tag{25}$$

Since eigenvalue of full system $\lambda = -ikc$

$$\begin{aligned} c = \frac{\lambda}{-ik} &= \frac{i\lambda_I + \lambda_r}{-ik} \\ &= \frac{1}{k}(\lambda_r i - \lambda_I) \end{aligned} \tag{26}$$

where λ_r and λ_I are real and imaginary part of eigenvalues. For netural modes, λ_I is zero, plug (26) into

(25) and after nondimensionalisation:

$$\underbrace{(Kz+\lambda_I)}_{\text{i}}\underbrace{[-K^2\phi+\frac{\partial^2\phi}{\partial z^2}]}_{\text{ii}}=0 \tag{27}$$

(ii) in is the part solved by reduced system and previous analytical solution for growth rate. However, when $z=-\frac{\lambda_I}{K}$, governing equation for interior fluid can also be satisfied.

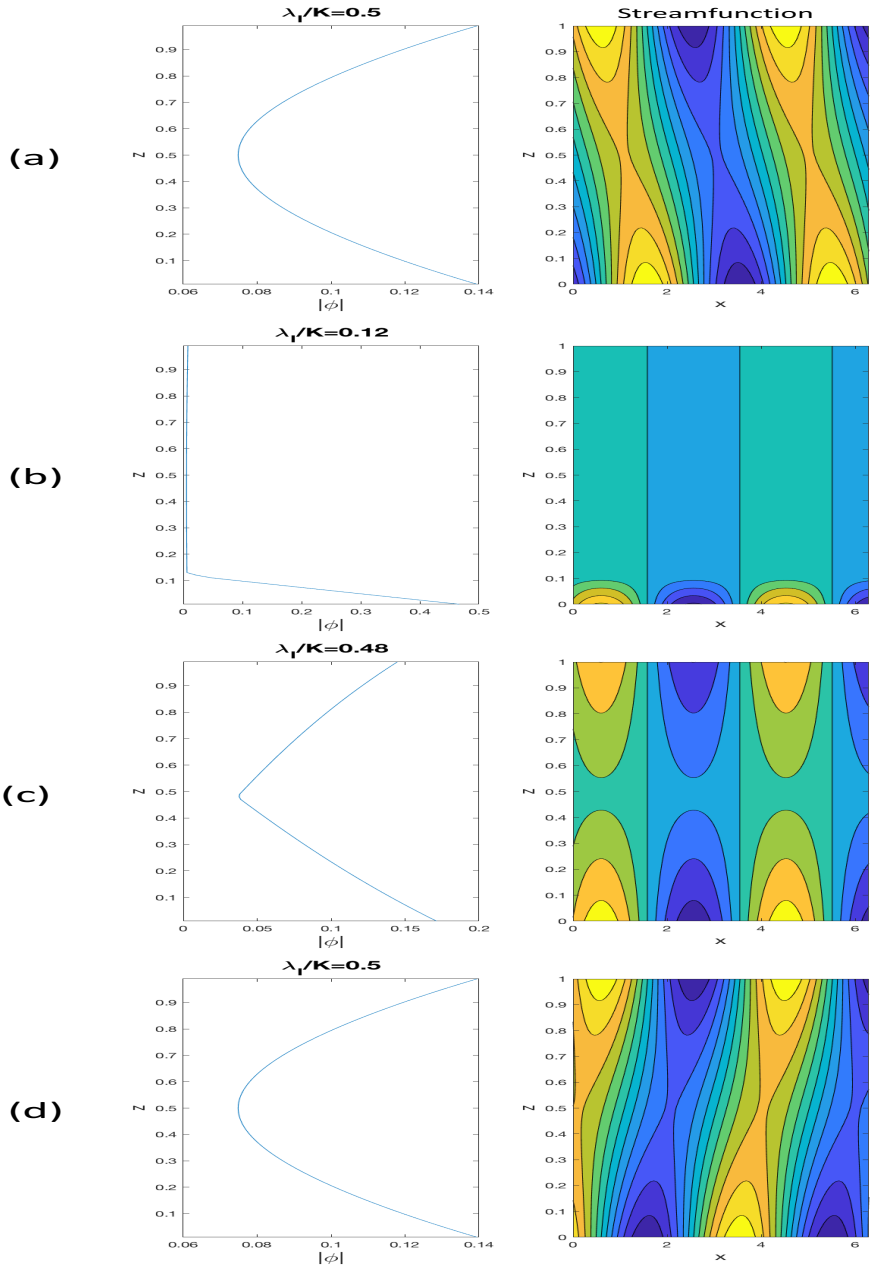

Figure 18: Eigenmodes of full system for K=1.6 (a) unstable mode (b) and (c) netural modes (d) stable mode

Fig 18 displays eigenmodes of full system. Left column is profiles $|\phi(z)|$ for different modes with (a) unstable mode and (d) stable mode. (c) and (d) are two of netural modes corresponding to some two points in the straight line shown in Fig. 17. It can be seen that profiles for stable and unstable mode are smooth. For netural modes, $\phi(z)$ is not differentiable at $z = -\lambda_I/K$. Therefore, netrual modes satisfy (i) in (27) instead of (ii). In addition, imagery part of eigenvalues for both stable and unstable mode are 0.5, i.e. the phase speed is 0.5, which is consistent with interpretation of edge waves.

There are infinite netural modes like Fig. 18 (b) and (c) in full system in both modally unstable (Fig. 17 (a)) and modally stable(Fig. 17 (b)). When we excite this full system with optimal initial conditions, it linearly combines these eigenmodes, producing structures shown in Fig. 12 and Fig. 16 which are totally different from the pattern of stable and unstable mode. Since $\mathbb{A}$ is non-normal, these modes are not orthogonal, therefore they will interact with each other, generating transient energy growth. Whereas the reduced system only has two modes to combine with, hence the structure of optimal initial conditions are always similar with those two modes and the transient energy growth is much smaller than that in full system.

References

[Emanuel(2009)] Kerry Emanuel. Quasi-balanced circulations in oceans and atmospheres. `https://ocw.mit.edu/courses/earth-atmospheric-and-planetary-sciences/12-803-quasi-balanced-circulations-in-oceans-and-atmospheres-fall-2009/`, 2009.

[Farrell and Ioannou(1996)] Brian F Farrell and Petros J Ioannou. Generalized stability theory. part i: Autonomous operators. *Journal of the atmospheric sciences*, 53(14):2025–2040, 1996.

[Simpson(2011)] Isla Simpson. Atmospheric dynamics. `http://www.cgd.ucar.edu/staff/islas/teaching/PHY2504HS.html`, 2011.

[Vallis(2017)] Geoffrey K. Vallis. *Barotropic and Baroclinic Instability*, page 335?378. Cambridge University Press, 2 edition, 2017. doi: 10.1017/9781107588417.010.